

# Resolving the Host Galaxy of the Nearby QSO I Zw 1 with Sub-Arcsecond Multi-Transition Molecular Line Observations<sup>1,2</sup>

J.G. Staguhn<sup>3,4,5</sup>, E. Schinnerer<sup>6,7</sup>, A. Eckart<sup>8</sup>, J. Scharwächter<sup>8</sup>  
 staguhn@stars.gsfc.nasa.gov

## ABSTRACT

We present the first sub-kpc ( $\sim 0.7'' \approx 850$  pc) resolution  $^{12}\text{CO}(1-0)$  molecular line observations of the ISM in the host galaxy of the QSO I Zw 1. The observations were obtained with the BIMA mm-interferometer in its compact A configuration. The BIMA data are complemented by new observations of the  $^{12}\text{CO}(2-1)$  and  $^{13}\text{CO}(1-0)$  line with IRAM Plateau de Bure mm-interferometer (PdBI) at  $0.9''$  and  $1.9''$  resolution, respectively. These measurements, which are part of a multi-wavelength study of the host galaxy of I Zw 1, are aimed at comparing the ISM properties of a QSO host with those of nearby galaxies as well as to obtain constraints on galaxy formation/evolution models. Our images of the  $^{12}\text{CO}(1-0)$  line emission show a ring-like structure in the circumnuclear molecular gas distribution with an inner radius of about 1.2 kpc. The presence of such a molecular gas ring was predicted from earlier lower angular resolution PdBI  $^{12}\text{CO}(1-0)$  observations. A comparison of the BIMA data with IRAM PdBI  $^{12}\text{CO}(2-1)$  observations shows variations in the excitation conditions of the molecular gas in the innermost  $1.5''$  comprising the nuclear region of I Zw 1. The observed properties of the molecular cloud complexes in the disk of the host galaxy suggest that they can be the sites of massive circumnuclear star formation, and show no indications of excitation by the nuclear AGN. This all indicates that the molecular gas in a QSO host galaxy has similar properties to the gas observed in nearby low luminosity AGNs.

*Subject headings:* galaxies: ISM, nuclei—quasars: individual (I Zw 1)

<sup>1</sup>Based on observations carried out with the Berkeley Illinois Maryland Association (BIMA) observatory. The BIMA observatory is supported by NSF grant AST-9981289

<sup>2</sup>Based on observations carried out with the IRAM Plateau de Bure Interferometer. IRAM is supported by INSU/CNRS (France), MPG (Germany) and IGN (Spain)

<sup>3</sup>NASA/Goddard Space Flight Center, Greenbelt, MD 20771, USA

<sup>4</sup>Department of Astronomy, University of Maryland, College Park, MD 20742, USA

<sup>5</sup>SSAI, Lanham, MD 20706, USA

<sup>6</sup>NRAO, Socorro, NM 87801, USA

<sup>7</sup>Jansky Postdoctoral Fellow at the National Radio Astronomy Observatory

<sup>8</sup>1. Physik. Inst., Univ. zu Köln, 50923 Köln, Germany

## 1. Introduction

One of the open questions in galaxy evolution is concerned with the formation of active galactic nuclei (AGN) and its relation to star formation (SF) in early type galaxies. The separation of starburst and AGN components in extragalactic objects – especially in host galaxies of quasars and QSOs – is a key problem in the investigation of evolutionary sequences proposed for AGNs (Norman & Scoville 1988; Sanders et al. 1988; Rieke et al. 1988; Haas et al. 2003). Although it is not exactly known how the host galaxy affects the energy release of the QSO, there is statistical evidence for preceding mergers or current interaction of QSO host galaxies with a companion galaxy (McLeod & Rieke 1994; Lim & Ho 1999). It is believed that quasar activity is a common, but short

lived, phenomenon in galaxy evolution (McLeod et al. 1999). Furthermore, host galaxies of QSOs show enhanced SF activities (Courvoisier 1998). The transition between Ultra Luminous Infrared Galaxies (ULIRG) and AGN seems to be continuous, all showing signs of enhanced star formation in their nuclear regions (Genzel et al. 1998; McLeod et al. 1999).

Millimeter molecular line observations are ideal for studying the mechanisms which transport the molecular gas into the AGN. Observations of abundances, excitation and dynamics of the molecular interstellar medium in the central regions of AGN are essential, since the interstellar matter provides the "fuel" for star formation as well as the central engine. Consequently, there are large numbers of high resolution observations available for nearby objects. These observations have revealed the presence of circumnuclear starburst rings in a large number of (nearby) active and IR luminous galaxies (e.g. NGC 1068, Planesas et al. 1991; NGC7469, Genzel et al. 1995; BIMA SoNG, Helfer et al. 2003). The extension of high angular resolution observations of molecular gas emission lines to QSO hosts is imperative in order to understand the connection between local active galaxies and high- $z$  QSOs. The results can be used to refine model predictions of the physical conditions in high  $z$ - QSOs (such as used e.g. in Combes et al. 1999).

Due to the limited angular resolution of single dish mm-wavelength telescopes, only interferometric observations at these wavelengths allow insight into the morphology and into the kinematics of molecular clouds in the nuclear region of QSO host galaxies with sufficient angular resolution. High resolution molecular line observations allow for detailed kinematic studies of the cold interstellar medium and the derivation of important parameters such as gas masses, surface mass densities and star formation efficiencies. Observations of multiple CO transitions reveal excitation conditions and thus can be used to constrain the physical conditions in an observed region. They can be used to better constrain the contribution of star formation to the total observed infrared luminosities.

### 1.1. The nearby QSO I Zw 1

The radio-quiet QSO I Zw 1 is regarded as the closest QSO which can be used for detailed studies of its host galaxy (Tab. 1). I Zw 1 has a systemic velocity of  $18,290 \text{ km s}^{-1}$ , which corresponds to a redshift of 0.0611 (Condon et al. 1985), or a distance of 255 Mpc ( $h_0 = 0.72$ , Spergel et al. 2003). The nucleus of I Zw 1 is extremely bright in the optical ( $M_B$  of -23.45 mag, Schmidt & Green 1983; Barvainis et al. 1989) and also has very bright X-ray emission (Krupe et al. 1990). I Zw 1 belongs to the class of infrared luminous galaxies ( $L_{FIR} = 10^{11.3} L_\odot$ , Haas et al. 2003), however its QSO nature is not apparent in the FIR. There is a strong indication for interaction between I Zw 1 and a neighboring companion (e.g. Lim & Ho 1999; Scharwächter et al. 2003).

A direct comparison between the FIR emission and CO molecular line emission in the host galaxy reveals that the FIR continuum emission of I Zw 1 is predominantly thermal in nature (Barvainis et al. 1989). The FIR to  $^{12}\text{CO}(1-0)$  ratio shows a star formation efficiency of about  $30 L_\odot/M_\odot$  in the nuclear region (Eckart et al. 1994). Schinnerer et al. (1998) show that the molecular gas mass in the central  $3.3''$  (3.7 kpc) is  $2/3$  of the total observed mass of  $9 \times 10^9 M_\odot$ . A kinematic analysis of their  $1.9''$  resolution PdBI  $^{12}\text{CO}(1-0)$  observations suggests that the central molecular gas is distributed in a ring of  $1.5''$  ( $\sim 1.9$  kpc) diameter. However the observations do not spatially resolve this ring. High resolution NIR observations show that the nuclear NIR spectrum is dominated by emission from the AGN, nevertheless about 25% of the NIR emission can be attributed to a nuclear starburst (Schinnerer et al. 1998), which might be located in the molecular gas ring. The star formation activity in the host galaxy of I Zw 1 underlines the important role of starbursts in the evolution of QSOs.

Only sub-arcsecond molecular line observations would allow actual imaging of this possible starburst ring. The extension of BIMA's longest baselines up to a maximum of almost 2 km makes the array the millimeter instrument with the highest angular resolution currently available. Here we present  $^{12}\text{CO}(1-0) \sim 0.7''$  angular resolution observations of the QSO I Zw 1. This corresponds to a spatial resolution of roughly 850 pc. We also

present new observations with the IRAM PdBI in  $^{12}\text{CO}(2-1)$  and  $^{13}\text{CO}(1-0)$  line at  $0''.9$  and  $2''.1$  resolution, respectively.

## 2. Observations and data reduction

### 2.1. BIMA observations

The data presented here were taken in December 1999 in the compact A array configuration (A-) of the ten element BIMA array (Welch et al. 1996) with baselines between 80 and 1310 m. Four more tracks of A array observations were obtained in February 2000, December 2001, and January 2002, but all of those yielded only poor quality data, demonstrating that this project poses requirements which are at the limit of what can be done with long baseline mm-interferometry to date. The digital correlator was configured to cover two 800 MHz bands with the upper sideband centered at the redshifted  $^{12}\text{CO}(1-0)$  frequency of 108.633 GHz. The sky opacity is significantly lower at the frequency of redshifted  $^{12}\text{CO}(1-0)$  transition than at the rest frequency. System temperatures during the observations ranged from 180 to 400 K, single-sideband. We flagged data such that most observations with system temperatures above 300 K were rejected. The data were reduced with the MIRIAD software package (Sault et al. 1995).

The fluctuations in the atmosphere follow a Kolmogorov power law distribution up to the maximum baseline of 2 km in the A array configuration of the BIMA array. This means that phase variations increase with baseline length, and therefore long baseline observations require a particularly careful phase calibration. We employed fast phase referencing: the observations were switched between the source, the phase calibrator (0108+015, distance from I Zw 1  $\sim 11^\circ$ ) and an additional point source, the quasar 0121+118 (angular distance from I Zw 1  $\sim 7^\circ$ ) which serves as a test source to determine the accuracy of the solutions for the phases. One complete cycle takes less than two minutes in order to follow closely the atmospheric phase (Holdaway & Owens 1993).

The test calibrator was used to select the best quality data: only observing cycles for which the test source maps to a point source down to the 20% level of its peak flux were selected (Fig. 1). This criterion was chosen to allow for a good qual-

ity image of the source. The reverse check, using 0121+118 as phase calibrator and 0108+015 as the test source, verified that the phase solutions derived from the test calibrator are of the same accuracy. Only the data taken in December 1999 have sufficient phase coherence to yield sub-arcsecond resolution observations. The data presented here are only from this observing track. The phase solutions derived from the test source 0121+118 were used for the images shown here, since this source is closer to I Zw 1 and therefore provides the best phase coherence. 0121+118 has a very flat spectrum with a flux of 1.1 Jy at 3.7 cm, 2 cm, and 7 mm (VLA calibrator list) and we use the same value for our 3 mm band. We estimate the uncertainty in the amplitude calibration to be better than 30%. In order to increase the signal to noise ratio in the data, we smoothed them to an effective angular resolution of  $0.7''$ .

### 2.2. IRAM PdBI observations

I Zw 1 was observed simultaneously in the  $^{12}\text{CO}(2-1)$  and  $^{13}\text{CO}(1-0)$  line in August 1996 with the four-element IRAM Plateau de Bure millimeter interferometer (PdBI) in the C configuration. Further dual-frequency observations in the B configuration were obtained in January 1997 and January/February 1998 with the then five-element array. The correlator was centered on the redshifted  $^{12}\text{CO}(2-1)$  frequency of 217.26321 GHz at 1 mm and the redshifted  $^{13}\text{CO}(1-0)$  frequency of 103.85578 GHz at 3 mm. With baselines between 40 and 280 m the data have a spatial resolution of  $\sim 0.86''$  with uniform weighting for the  $^{12}\text{CO}(2-1)$  line (Fig. 2), and  $\sim 2.1''$  with natural weighting for the  $^{13}\text{CO}(1-0)$  line. The noise per  $20(40)$  km  $\text{s}^{-1}$  wide channel is  $1.7(0.33)$  mJy  $\text{beam}^{-1}$  in the combined data for the  $^{12}\text{CO}(2-1)(^{13}\text{CO}(1-0))$  line. The quasar 3C454.3 served as a passband calibrator, while standard IRAM PdBI phase calibrators were observed every 20 minutes. The data were calibrated and mapped using the IRAM GILDAS software package (Guilloteau & Lucas 2000).

## 3. Results

### 3.1. Spatial distribution of the $^{12}\text{CO}(1-0)$ line emission

The gas disk of I Zw 1 is clearly resolved in its  $^{12}\text{CO}(1-0)$  line emission at  $0.7''$  resolution (Fig.

TABLE 1  
ADOPTED PROPERTIES OF I ZW 1 (=PG0050+124)

Property	Value
Right ascension (J2000.0)	00 <sup>h</sup> 53 <sup>m</sup> 34 <sup>s</sup> .9
Declination (J2000.0)	+12°41'36".2
Inclination (deg)	38
Position angle (deg)	135
Systemic velocity (km s <sup>-1</sup> )	18,290
Distance (Mpc)	255
1"	1.24 kpc

-The coordinates refer to the phase center of the millimeter observations. The inclination and position angle are taken from Schinnerer et al. (1998), while the systemic velocity is from Condon et al. (1985).

TABLE 2  
I ZW 1 <sup>12</sup>CO(1-0) BEAM AVERAGED PARAMETERS

Region	$\Delta v$ [km s <sup>-1</sup> ]	$T_B$ [K]	$I_{CO}$ [K km s <sup>-1</sup> ]	$N_{H_2}$ [10 <sup>21</sup> cm <sup>-2</sup> ]
Disk (9.0") <sup>a</sup>	310	0.03	10	2
Nucleus (2.0")	400	1.8	720	144
kpc ring (0.7")	100	12	1200	240

<sup>a</sup>from Schinnerer et al. (1998)

3). These are the first molecular line observations which resolve the emission in the nuclear region and show that the emission is not centrally peaked: the strongest molecular line emission is not coincident with the optical center of the galaxy, but situated at a distance between  $1''$  and  $3''$ , mainly to the South and East of the galaxy center. This corresponds to a distance of between 1.2 kpc and 3.7 kpc from the nucleus. This emission, which occurs at positive offsets in R.A. with respect to the major axis, has predominantly positive velocities (see position-velocity ( $pv$ ) diagram in Figure 4). When the velocity integrated BIMA  $^{12}\text{CO}(1-0)$  data are smoothed to a resolution of  $2''$  (Fig. 5, top left), which corresponds to the resolution of the corresponding  $^{12}\text{CO}(1-0)$  PdBI observations (Fig. 5, top right), we find a positional offset of  $\sim 1''$  in the center of emission of both images with respect to each other. The measured peak flux in the BIMA image, which is smoothed to a resolution of  $2''$  (Fig. 5, top left), is  $28 \text{ mJy beam}^{-1}$  or  $11 \text{ Jy beam}^{-1} \text{ km}^{-1} \text{ s}$ , slightly larger than the  $^{12}\text{CO}(1-0)$  peak flux of  $8 \text{ Jy beam}^{-1} \text{ km}^{-1} \text{ s}$ , at the same angular resolution observed with the PdBI. The difference of  $\sim 38\%$  is still within the expected range, if we assume an uncertainty of the PdBI calibration of 20%.

This significant spatial offset of the  $^{12}\text{CO}(1-0)$  center of emission in the BIMA and PdBI observations can not be due to a pointing error of the BIMA observations, since a pointing error of this magnitude is not visible in the image of the test quasar (Fig. 1). The fact that the negative velocity components in the BIMA observations (Fig. 4) are less pronounced than in the lower resolution PdBI data (Fig. 6, left) indicates that the molecular emission at these velocities has a more extended distribution and therefore is partially resolved out in the high resolution BIMA data. This effect naturally explains the shift of the observed center in the BIMA data. Probably the most convincing indication that the denser, and therefore probably more spatially confined, molecular clouds are situated to the South-East of the nucleus comes from the  $^{13}\text{CO}(1-0)$  observations we obtained with the PdBI (Fig. 5, bottom left): the center of emission in these data is also shifted towards the South-East. It is worthwhile to note that the peak of the line emission in all CO transitions is shifted by  $\sim 1''$  to the South-East of the nominal optical

center. This could be due to the fact that the distribution of the CO line intensity is asymmetric with respect to the AGN. This assumption could be tested if the position of the dynamical center could be accurately determined; however, even the resolution of our  $^{12}\text{CO}(2-1)$  data is not adequate to do so.

### 3.2. Properties of the molecular gas

The observed  $pv$  diagram along the major axis at  $0.7''$  resolution (Fig. 4) shows a circular rotation which is consistent with the lower resolution PdBI  $^{12}\text{CO}(1-0)$  observations (Fig. 6, left; see also Scharwächter et al. 2003). The consistency of the observed  $p - v$  diagrams in the BIMA and PdBI observations strongly supports the interpretation that the spatial offset of the peak emission in the BIMA image is not an artifact due to calibration errors. The peak emission of  $35 \text{ mJy beam}^{-1}$  in the BIMA  $pv$  diagram, which is observed over a velocity interval of about  $100 \text{ km s}^{-1}$ , corresponds to an average brightness temperature of  $T_B = 12 \text{ K}$  in this velocity interval. This indicates a large beam filling factor, respectively a significant amount of molecular gas within a region of  $600 \text{ pc}^2$ . Schinnerer et al. (1998) show that the standard conversion factor  $N(\text{H}_2)/I(\text{CO}) = 2 \times 10^{20} \text{ cm}^{-2} \text{ K}^{-1} \text{ km}^{-1} \text{ s}$  can be applied to the observed  $^{12}\text{CO}(1-0)$  line emission from I Zw 1.

The peak flux of  $18 \text{ mJy beam}^{-1}$  in the velocity integrated  $0.7''$  resolution image (Fig. 3) translates into a molecular hydrogen column density of  $4.9 \times 10^{23} \text{ cm}^{-2}$ . About 50% of this emission has a velocity consistent with its origin being in a circumnuclear ring at a distance of  $\sim 1.5''$ . The corresponding column density of  $2.4 \times 10^{23} \text{ cm}^{-2}$  in the molecular ring is two orders of magnitude larger than the average molecular gas column density of  $2 \times 10^{21} \text{ cm}^{-2}$  in the disk region, and roughly a factor of two larger than the average column density of  $1.4 \times 10^{23} \text{ cm}^{-2}$  in the nuclear region (the innermost  $2''$  region: see Table 2 for a summary of the observed  $^{12}\text{CO}(1-0)$  molecular line properties).

### 3.3. Multi-transition analysis of the molecular line emission

Our PdBI observations of the  $^{12}\text{CO}(2-1)$  and  $^{13}\text{CO}(1-0)$  line detect an integrated line flux  $I_{\text{CO}}$

of  $18 \text{ Jy km s}^{-1}$  and  $0.5 \text{ Jy km s}^{-1}$ , respectively. Thus they recover only about 30% (15-20%) of the observed IRAM 30m single dish flux of  $61 \text{ Jy km s}^{-1}$  ( $3.1 \text{ Jy km s}^{-1}$ ) for the  $^{12}\text{CO}(2-1)$  ( $^{13}\text{CO}(1-0)$ ) line (Eckart et al. 1994). In contrast to the BIMA  $^{12}\text{CO}(1-0)$  observations, the  $0.86''$  resolution PdBI  $^{12}\text{CO}(2-1)$  observations (Fig. 5, bottom right) do not show any particular spatial structure in the nuclear region. This discrepancy can only be explained by a difference in the excitation of the molecular gas in the nucleus (innermost  $1''$ ) and the emission from molecular clouds which are situated further out. This interpretation is supported by both the PdBI and BIMA  $^{12}\text{CO}(1-0)$  observations: A comparison of the  $pv$  diagrams from the PdBI  $^{12}\text{CO}(1-0)$  observations from Schinnerer et al. (1998) (here chosen for the better signal to noise) and our new PdBI  $^{12}\text{CO}(2-1)$  and  $^{13}\text{CO}(1-0)$  observations can be seen in Figure 6. The peaks of the line intensity are shifted from  $\pm 150 \text{ km s}^{-1}$  in the  $^{12}\text{CO}(1-0)$  line to lower velocities of  $\pm(50 - 100) \text{ km s}^{-1}$  in the  $^{12}\text{CO}(2-1)$  line. This difference becomes even more obvious in the  $R_{21} = \frac{^{12}\text{CO}(2-1)}{^{12}\text{CO}(1-0)}$  line peak ratio map of the major kinematic axis  $pv$  diagram shown in Figure 7. For these ratios the resolution of the  $^{12}\text{CO}(2-1)$  observations was smoothed to match the PdBI  $^{12}\text{CO}(1-0)$  observations. The line peak brightness ratio in the inner  $\sim 1.5''$  of I Zw 1 is  $\approx 0.5$ . This drops by almost a factor of two to  $\approx 0.3$  at the position of the  $^{12}\text{CO}(1-0)$  line peaks at  $\pm 150 \text{ km s}^{-1}$ . This suggests that the outer  $^{12}\text{CO}(1-0)$  clouds, which are apparently not resolved out by the BIMA observations with a similar angular resolution as the PdBI  $^{12}\text{CO}(2-1)$  observations, are more subthermally excited than the molecular gas in the innermost region of I Zw 1. The fact that the denser and more thermalized molecular material breaks up into several distinct velocity components in the  $^{12}\text{CO}(2-1)$  emission (Figure 6) strongly suggests that circumnuclear star formation and not the central AGN is exciting the molecular line emission.

The derived  $r_{10} = \frac{^{12}\text{CO}(1-0)}{^{13}\text{CO}(1-0)}$  line peak brightness ratio for the three  $^{13}\text{CO}(1-0)$  line peaks above  $3\sigma$  (see Figure 6, right) is about 15. This value can probably be regarded only as an upper limit due to the large amount of missing flux which has been resolved out by our interferometric observations, in particular in the  $^{13}\text{CO}(1-0)$  observations (see above). We therefore avoid further interpretation

of these ratios.

NIR spectra of the inner  $3.3''$  of I Zw 1 indicate the presence of circumnuclear star formation (Schinnerer et al. 1998). The millimeter line ratios for the inner  $1.5''$  suggest that these GMCs could be the site of this massive star formation. However, the BIMA observed  $^{12}\text{CO}(1-0)$  GMCs, which are further out, are also likely candidates for the observed starburst due to their high column densities. A starburst in these clouds might be triggered by the interaction of I Zw 1 with the companion galaxy (see Scharwächter et al. 2003).

### 3.4. Molecular gas kinematics

There is some enhanced emission in the BIMA  $pv$  diagram (Fig. 4) at velocities which are "forbidden" with respect to circular motion, most prominently at a positive angular offset of  $2''$  along the major axis between  $-40$  and  $-60 \text{ km s}^{-1}$ . Other than the emission from the circular rotation, it is pronounced only in one bin of the  $p-v$  diagram, and with a signal to noise ratio of  $4\sigma$  its significance is not sufficient to be considered a clear detection. The  $^{12}\text{CO}(2-1)$  velocity field (Fig. 8) also shows indications of deviation from pure circular rotation for radii of  $r \geq 1''$ , as is evident in the change in the line of nodes. Due to the lack of emission, this potential non-circular motion can not be followed to larger radii. Together with the "forbidden"  $^{12}\text{CO}(1-0)$  it can be seen as circumstantial evidence that some transportation mechanism for the molecular gas is active in the disk of I Zw 1. However, data of higher angular resolution and improved sensitivity will be needed to confirm this. A more detailed analysis of the observed rotational pattern can be found in Scharwächter et al. (2003).

## 4. Summary and Conclusions

Our BIMA  $^{12}\text{CO}(1-0)$  observations represent the first molecular line observations of the host galaxy of a QSO with sub-kpc resolution. The molecular gas disk of a QSO is for the first time spatially resolved into individual giant molecular cloud complexes. We observe giant molecular clouds with peak molecular hydrogen column densities of  $2.4 \times 10^{23} \text{ cm}^{-2}$  at a distance between  $1''$  and  $3''$  from the nucleus. With such high column densities these clouds could be actively forming

stars.

The combination of BIMA observations with new and previously published PdBI CO data allows for the first interferometric multi-transition study in the disk of I Zw 1. The line brightness ratios in the inner 1.5'' are consistent with moderately dense cold GMCs, and they are not peaked at the center. This strongly suggests that the AGN has no significant effect on the central molecular material.

The exact location of the circumnuclear starburst very likely seen in nuclear NIR spectra (Schinnerer et al. 1998) is still not identified. Possible candidates are the resolved  $^{12}\text{CO}(1-0)$  molecular clouds seen by BIMA as well as the more thermalized material traced by the higher line ratios inside the inner 1.5''. However, any of these molecular clouds are likely sites of a massive starburst which contributes to the observed far-infrared luminosity of  $L_{FIR} = 10^{11.3} L_{\odot}$ .

The distribution and properties of the molecular gas in the host galaxy of the nearby QSO I Zw 1 are quite similar to what is observed in nearby low luminosity AGNs (e.g. Paglione et al. 2001; NUGA Survey, Garca-Burillo et al. 2003). This suggests that the ISM in QSO at high redshift might be similar to nearby low luminosity AGN as well.

Four additional attempts to re-observe I Zw 1 in  $^{12}\text{CO}(1-0)$  with BIMA in the A configuration all failed to provide useful data, due to insufficient phase coherence of the observations. This demonstrates that the observations presented here are on the limit of what can be done without active phase correction systems, at least from a site such as Hat Creek where the BIMA array is situated.

We would like to thank P.J. Teuben for his helpful advice with the data reduction. The constructive comments from the anonymous referee are much appreciated. A. Eckart. and J. Scharwächter are supported by DFG grant SFB 494. J. Scharwächter is also supported by a scholarship for doctoral students of the Studienstiftung des deutschen Volkes.

## REFERENCES

Barvainis,R., Alloin,D., and Antonucci,R. 1989, ApJ, 337L, 69

Combes,F., Maoli,R., and Omont,A. 1999, A&A, 345, 369

Condon, J.J, Hutchings, J.B., Gower, J.C. 1985, AJ, 90, 1642)

Courvoisie, T.J.L. 1998, ARA&A, 9, 1

Eckart,A., vanderWerf,P.P., Hofmann,R., and Harris,A.I. 1994, ApJ, 424, 627

Garca-Burillo, S., Combes, F., Hunt, L. K., Boone, F., Baker, A. J., Tacconi, L. J., Eckart, A., Neri, R. 2003, A&A407, 485 Leon, S.; Schinnerer, E.; Englmaier, P.

Genzel, R., Weitzel, L., Tacconi-Garman, L. E., Blietz, M., Krabbe, A., Lutz, D., and Sternberg, A. 1995, ApJ, 444, 129

Genzel,R., Lutz,D., Sturm,E., Egami,E., Kunze,D., Moorwood,A.F.M., Rigopoulou,D., Spoon,H.W.W., Sternberg,A., Tacconi-Garman,L.E., Tacconi,L., and Thatte,N. 1998, ApJ, 498, 579

Guilloteau, S., Lucas, R. 2000, in Imaging at Radio through Submillimeter Wavelengths, ed. J.G. Mangum, S.J.E. Radford, ASP Conf. Ser., 299

Haas,M., Klaas,U., Mller,S.A.H., Bertoldi,F., Camenzind,M., Chini,R., Krause,O., Lemke,D., Meisenheimer,K., Richards,P.J., Wilkes,B.J. 2003, A&A, 402, 87

Helfer, T.T., Thornley, M.D., Regan, M.W., Wong, T., Sheth, K., Vogel, S.N., Blitz, L., Bock, D.C.-J. 2003, ApJS, 145, 259

Holdaway, M.A., and Owens, F.N. 1993, ALMA Memo Series, 126

Kruper,J.S., Canizares,C.R., and Urry,C.M. 1990, ApJS, 74, 347

Lim,J., and Ho,P.T.P 1999, ApJ, 510, 7

McLeod,K.K., and Rieke,G.H. 1994, ApJ, 431, 137

McLeod,K.K., Rieke,G.H., and Storrie-Lombardi,L.J. 1999, ApJ, 511L, 67

Norman, C., and Scoville, N. 1988,ApJ, 332, 124

- Paglione, T.A. D., Wall, W. F., Young, J. S., Heyer, M. H.; Richard, M., Goldstein, M., Kaufman, Z., Nantais, J., and Perry, G. 2001, *ApJS*, 135 183
- Planesas,P., Scoville,N., and Myers,S.T 1991, *ApJ*, 369, 364
- Sanders, D. B., Soifer, B. T., Elias, J. H., Madore, B. F., Matthews, K., Neugebauer, G., and Scoville, N. 1988, *ApJ*, 325, 74
- Sault, R. J., Teuben, P. J., and Wright, M. C. H. 1995, *PASPConf. Ser.* 77, 433
- Scharwächter,J., Eckart,A., Pfalzner,S., Moul-taka,J., Straubmeier,C., and Staguhn,J.G. 2003, *A&A*, 405, 959
- Schinnerer,E., Eckart,A., and Tacconi,L.J. 1998, *ApJ*, 500, 147
- Schmidt,M., and Green,R.F. 1983, *ApJ*, 269, 352
- Spiegel, D.N., Verde, L., Peiris, H.V., Komatsu, E., Nolta, M.R., Bennett, C.L., Halpern, M., Hinshaw, G., Jarosik, N., Kogut, A., Limon, M., Meyer, S.S., Page, L., Tucker, G.S., Weiland, J.L., Wollack, E., and Wright, E. L. 2003, *ApJS*, 148, 175
- Rieke, G. H., Lebofsky, M. J., and Walker, C. E. 1988, *ApJ*, 325, 679
- Welch,W.J., et al. 1996, *PASP*, 108, 93

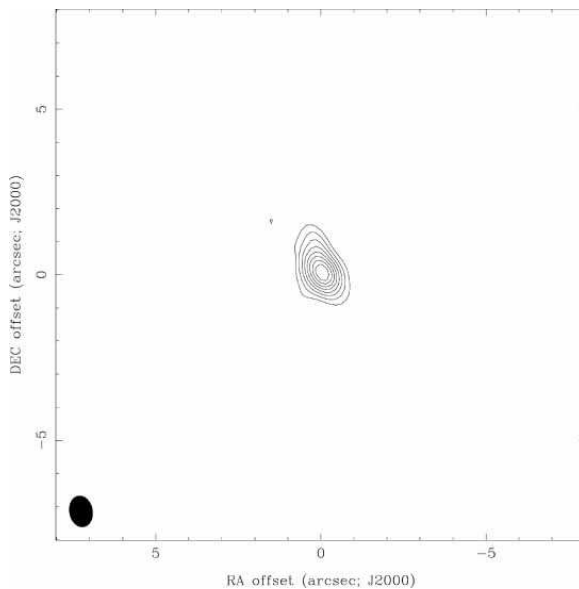


Fig. 1.— BIMA image of the test source 0121+118 in  $^{12}\text{CO}(1-0)$ . The contour lines start at 20% of the peak level in increments of 10%. Only the 20% contour shows a slight deviation from the ideal point source response. The synthesized beam is shown in the lower left of the image.



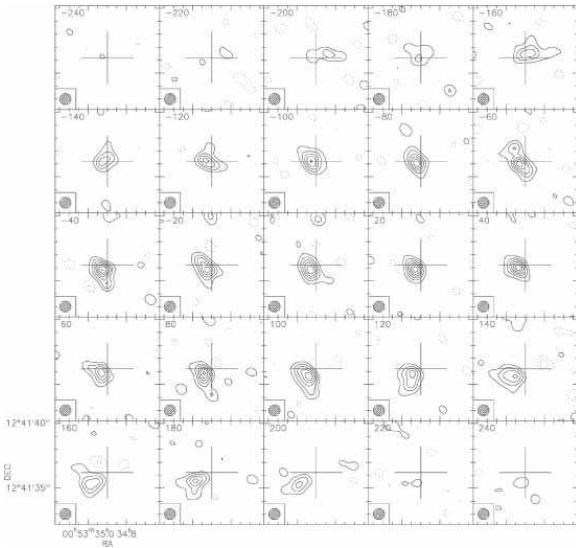


Fig. 2.— Channel maps of  $^{12}\text{CO}(2-1)$  line emission in I Zw 1 observed with the PdBI. The relative velocities with respect to the observed systemic velocity are indicated in the upper left corner of each panel. The data have a resolution of  $0.86''$  and the contours are in steps of  $5 \text{ mJy beam}^{-1}$  ( $\sim 3\sigma$ ). The rotation of the galactic CO disk is clearly evident in the channel maps. The clean beam is shown for reference in the lower left corner of each panel.

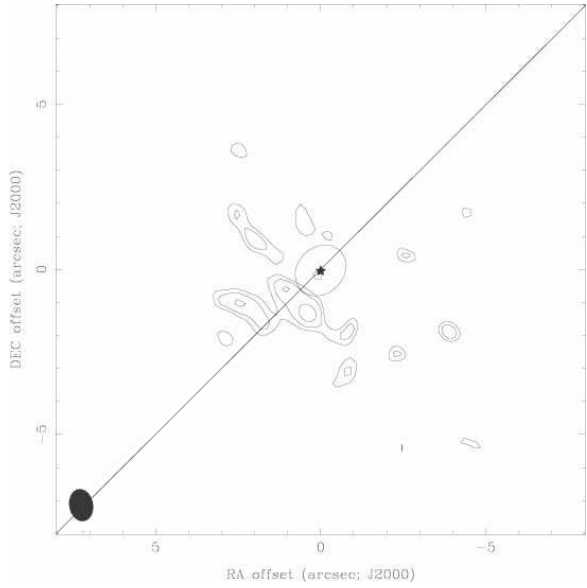


Fig. 3.— BIMA image of the  $^{12}\text{CO}(1-0)$  emission smoothed to a resolution of  $0.7''$ . The solid contours show the velocity integrated emission between  $-160$  and  $240 \text{ km s}^{-1}$  in  $1\sigma$  steps ( $3 \text{ mJy beam}^{-1}$ ) starting at  $4\sigma$  ( $9 \text{ mJy beam}^{-1}$ ). If present, dashed contours would represent the corresponding negative values for the flux density. The ellipse in the center of the image marks the projected distance of  $1 \text{ kpc}$  ( $0.8''$ ) from the center. The diagonal line indicates the major kinematic axis of the galaxy. The ellipse in the lower left corner shows the synthesized beam.

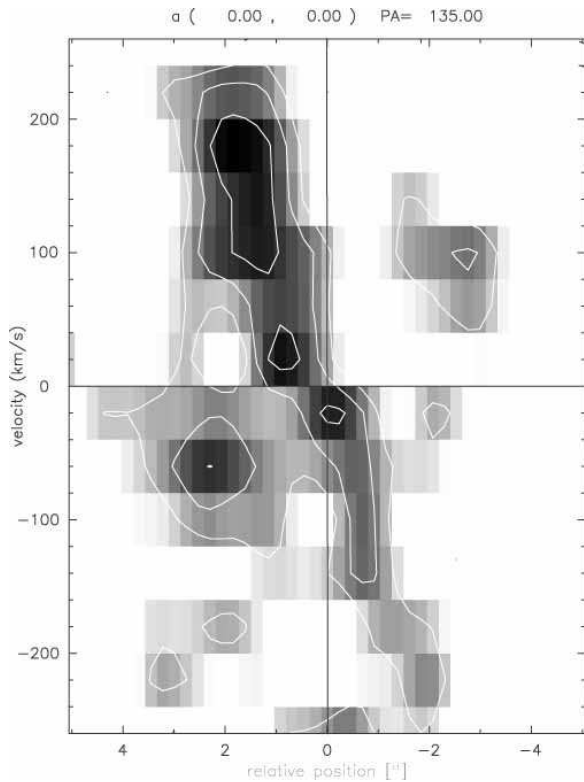


Fig. 4.— BIMA  $^{12}\text{CO}(1-0)$  position-velocity diagram along the major axis ( $135^\circ$ ) of I Zw 1 with a spatial resolution of  $0.7''$ . The contours start at 60% ( $3\sigma$ ) of the peak flux of  $35 \text{ mJy beam}^{-1}$  with increments of 15% ( $1\sigma$ ).

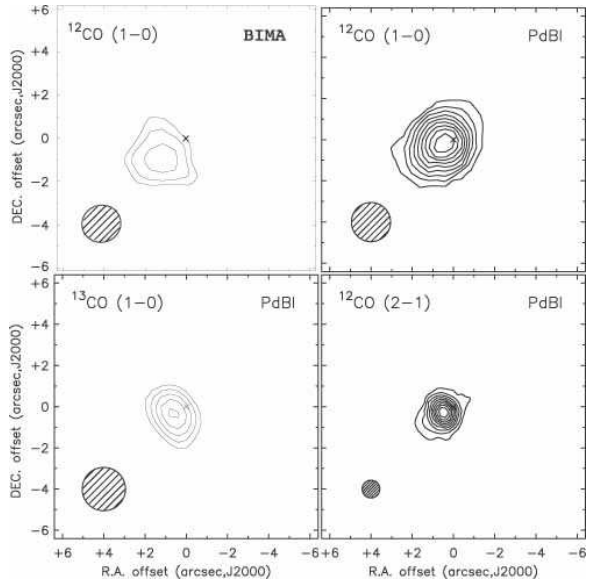


Fig. 5.— *Top left*: BIMA image of the  $^{12}\text{CO}(1-0)$  emission smoothed to a resolution of  $2.0''$ . The solid contours show the velocity integrated emission between  $-160$  and  $240 \text{ km s}^{-1}$  in  $1\sigma$  steps ( $4 \text{ mJy beam}^{-1}$ ) starting at  $4\sigma$  ( $17 \text{ mJy beam}^{-1}$ ). Dashed contours would show the corresponding negative values for the flux density, if it were present in the image. The ellipse in the lower left corner shows the synthesized beam. To obtain integrated line fluxes, these and the following values should be multiplied by the velocity range. *Top right*: PdBI  $^{12}\text{CO}(1-0)$  0th moment image with  $1.9''$  resolution, integrated between  $-240$  and  $+240 \text{ km s}^{-1}$ . The contours start at 10% of the peak flux of  $0.016 \text{ Jy beam}^{-1}$  and are in steps of 10%. *Bottom left*: PdBI  $^{13}\text{CO}(1-0)$  image integrated over the velocity range of  $-240$  and  $+240 \text{ km s}^{-1}$ . The contours are at  $0.3$  ( $3\sigma$ ),  $0.4$ ,  $0.5$ ,  $0.7$ , and  $0.8 \text{ mJy beam}^{-1}$  ( $7\sigma$ ). *Bottom right*: PdBI  $^{12}\text{CO}(2-1)$  0th moment image at  $0.86''$  resolution, integrated between  $-240$  and  $+240 \text{ km s}^{-1}$ . The contours start at 10% of the peak flux of  $0.017 \text{ Jy beam}^{-1}$  and are in steps of 10%. A cross marks the position of the optical center in each panel.

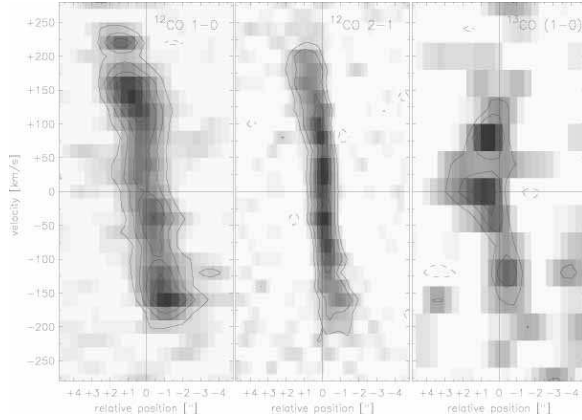


Fig. 6.— PdBI data  $pv$  diagrams along the major axis ( $135^\circ$ ) of I Zw 1. The  $^{12}\text{CO}(1-0)$  emission (*left*) is shown at  $1.9''$  resolution, the  $^{12}\text{CO}(2-1)$  emission (*middle*) at  $0.86''$  resolution and the  $^{13}\text{CO}(1-0)$  line emission (*right*) at  $2.1''$  resolution. The contours start at  $3\sigma$  in steps of  $3\sigma$  for the  $^{12}\text{CO}$  data with  $1\sigma = 2(1.7)$  mJy beam $^{-1}$  for the  $^{12}\text{CO}(1-0)$  ( $^{12}\text{CO}(2-1)$ ) line. For the  $^{13}\text{CO}(1-0)$  the contours start at  $2\sigma$  in steps of  $1\sigma$  with  $1\sigma = 0.3$  mJy beam $^{-1}$ .

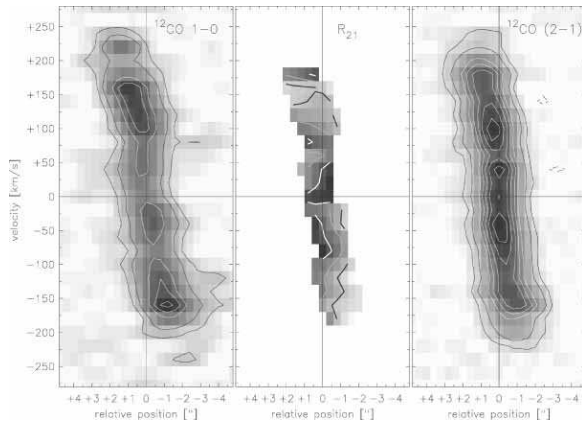


Fig. 7.— PdBI  $^{12}\text{CO}$  line  $pv$  diagrams at  $2.1''$  resolution. The  $R_{21} = \frac{^{12}\text{CO}(2-1)}{^{12}\text{CO}(1-0)}$  peak brightness ratio (*middle*) clearly shows a higher ratio in the inner  $1.5''$  which is decreasing by almost a factor of two towards higher velocities of  $\pm 150$  km s $^{-1}$ . The contours are at 0.3 (black line), 0.4 (grey line) and 0.5 (white line). For reference the  $^{12}\text{CO}(1-0)$  (*left*) and  $^{12}\text{CO}(2-1)$  (*right*)  $pv$  diagrams are shown at a resolution of  $2.1''$ . The contours start at  $3\sigma$  in steps of  $3\sigma$  with  $1\sigma$  of  $1.8$  mJy beam $^{-1}$ .

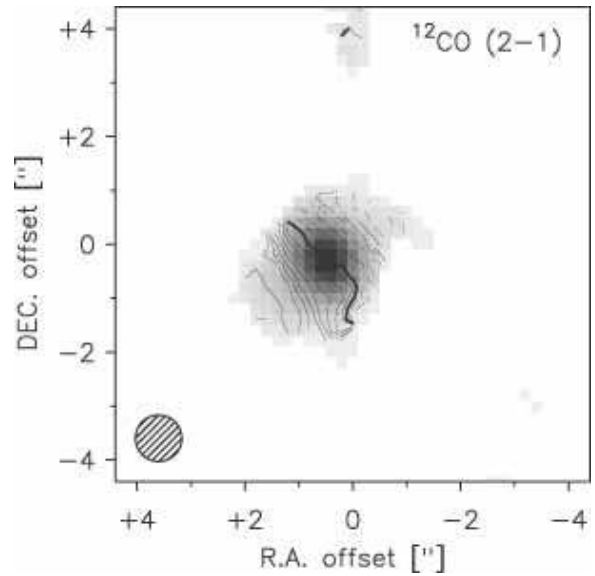


Fig. 8.— PdBI  $^{12}\text{CO}(2-1)$  velocity field at  $0.86''$  resolution. The velocity field is shown in contours (the thick line represents  $v_{hel} = 18,316$  km s $^{-1}$ , the solid (dashed) lines are positive (negative) velocities in steps of  $20$  km s $^{-1}$ ). The 0th moment image is shown in grayscale for comparison. The beam is indicated in the lower left corner.